JOURNAL OF GEOPHYSICAL RESEARCH, VOL. 105, NO. C2, PAGES 3401–3411, FEBRUARY 15, 2000

Current observations on the development of the Yellow Sea Warm Current

W. J. Teague and G. A. Jacobs

Naval Research Laboratory, Stennis Space Center, Mississippi

Abstract. Historically, the climatological mean northward flow in the Yellow Sea trough has been referred to as the Yellow Sea Warm Current (YSWC) since it was thought to originate as a branch of the Tsushima Current which transports warm Kuroshio waters. However, the Tsushima Current does not penetrate into the Yellow Sea interior during winter. The onset of what is referred to as the YSWC during winter is directly observed using measurements of current profiles, pressure, and temperature, and a wind climatology for the time period July 1995 through January 1996. The YSWC is a result of weak southerly winds during summer. During fall transition and winter monsoon periods, strong northerly wind bursts drive a north-to-south rise in pressure extending from the trough over to the Korean coast and force a northward flow in the Yellow Sea trough. The rise in pressure and corresponding north wind–forced YSWC begin at the end of October for this measurement period and are observed into January. These measurements show that the YSWC has different seasonal forcing mechanisms. Direct current measurements are also presented which suggest a current flow north of Cheju, sometimes referred to as the Cheju Warm Current.

1. Introduction

Currents in the Yellow Sea have proven difficult to predict and model. The general circulation is not well known. It is quite shallow, with depths ranging from ~90 m in an interior trough to ~20 m within 50 km of the coast. Seasonal variability of the circulation is expected to be large because of the shallow water depths and the extreme climate conditions related to the winter and summer monsoons. The circulation picture is further complicated during summer because of an influx of Yangtze River diluted water which has been observed as far east as Cheju [*Park*, 1986; *Beardsley et al*., 1985]. Prior to 1986 there were few measurements made on a basin-wide scale in the Yellow and East China Seas. Studies conducted separately by Korean, Chinese, and Japanese scientists were limited by territorial restrictions. Long-term direct current observations are very rare.

There is a northward, climatological mean flow along the Yellow Sea trough which has been referred to as the Yellow Sea Warm Current (YSWC) [*Nitani*, 1972]. First suggested by *Uda* [1934], a northward penetration of the YSWC into the Yellow Sea is considered representative of Yellow Sea circulation. Historically, this current has been identified as a branching of the Tsushima Current and is said to separate from either the Kuroshio [*Nitani*, 1972] or the Taiwan Warm Current [*Chen et al*., 1994; *Beardsley et al*., 1985] in the northeastern East China Sea. Either scenario would result in a transport of relatively warm and saline waters into the Yellow Sea. A tongue of warm water that often appears northwest of Cheju is frequently interpreted as a flow by the YSWC into the Yellow Sea [*Asaoka and Moriyasu*, 1966].

It is questionable as to whether the branching of the Tsushima Current known as the YSWC extrudes into the Yellow Sea interior. Some investigators have postulated that the northward current during the summer in the southeastern Yellow Sea is a density current formed between coastal waters and the Yellow Sea Cold Water [*Lie*, 1984] and is not a continuation of what is generally referred to as the YSWC. *Chen et al*. [1994] state that the branchings of the Taiwan Warm Current are not clearly documented near Cheju Island. However, analyses of hydrographic data obtained during summer suggest that the Kuroshio waters flow into the Cheju Strait after rounding the west coast of Cheju Island [*Park*, 1986]. In a more recent study a clockwise flow around Cheju has been observed using drifter observations by *Lie et al*. [1998] and has been called the Cheju Warm Current, since it is transporting warm and saline water. Furthermore, during winter, Kuroshio waters are not generally found north of Cheju [*Nakao*, 1977] although *Kondo* [1985] reported a northward extension of the YSWC into the Yellow Sea during winter from analysis of 13 years of temperature and salinity data. His results were not definitive during spring and summer. Evidence of northward flow in the Yellow Sea trough in winter has been found by *Hsueh* [1988]. He suggests that the YSWC is caused by north wind bursts during winter that result in a north-to-south sea surface slope while directly observing the demise of the northward flow during the spring transition in early March. Thus the YSWC may not be the result of a branching of the Tsushima Current.

To gain a better understanding of the YSWC response to wind forcing, direct current measurements in the Yellow Sea trough were made with three moored acoustic Doppler current profilers (ADCPs) with pressure gauges (PGs), during late summer and winter 1995. These arrays, deployed by the Naval Oceanographic Office, utilized newly designed "trawl resistant" instrument mounts since measurements of currents in the Yellow Sea interior are very difficult to obtain because of the intense level of fishing and trawling. Hence such measurements are relatively scarce. Emphasis here is on the onset of the YSWC. Current measurements at levels near the surface,

Paper number 1999JC900301.

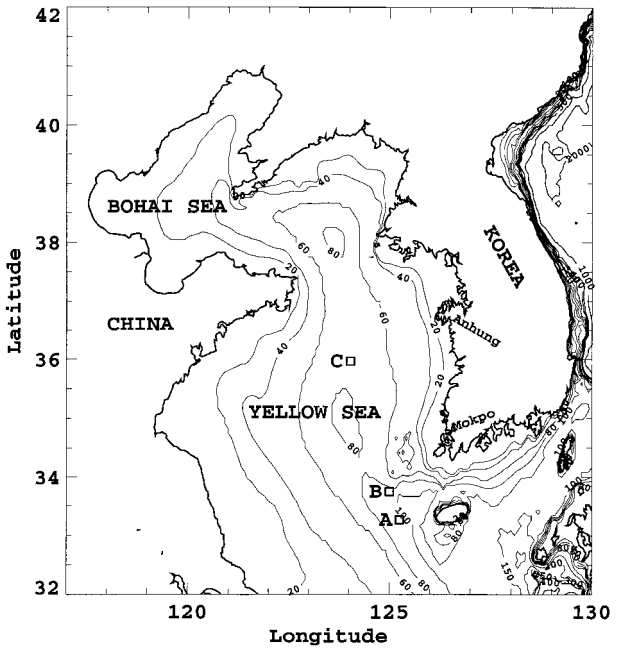

Figure 1. Bathymetry of the area and location of acoustic Doppler current profiler (ADCP) and pressure gauge moorings (A, B, and C; squares).

at middepth, and near the bottom are analyzed in conjunction with pressure and bottom temperature measurements obtained from the ADCP arrays, sea level measurements along the coast of Korea, winds from the Navy Operational Global Atmospheric Prediction System (NOGAPS) [*Hogan and Brody*, 1993; *Rosmond*, 1992; *Hogan and Rosmond*, 1991], and a temperature-salinity climatology. Evidence of the northward flow associated with the YSWC due to north wind bursts is found during fall, beginning at the end of October and continuing on into winter in addition to northward flow associated with southerly winds during summer.

2. Instrumentation

Conventional current meter arrays utilizing wire moorings cannot survive for any appreciable time in the Yellow Sea. Several of these conventional mooring types were deployed in the early 1990s by the U.S. Naval Oceanographic Office and did not survive, and hence a new mooring design utilizing ADCPs was implemented. The three moorings for this study, deployed by the U.S. Naval Oceanographic Office during July 1995, consisted of an ADCP (RD Instruments) and a PG (Sea-Bird Electronics Model 26, Seagauge). Each mooring used a trawl resistant bottom mount [*Cumbee and Foley*, 1995], which is a shallow dome-shaped enclosure that rests upon the bottom. The exposed side of the dome is relatively smooth in order to minimize snagging by fishing nets and lines. Instrumentation is safely enclosed within the dome ~1 m above the ocean bottom. Scraps of nets as well as evidence of trawl scrapings were found on the moorings at instrument retrieval. Surprisingly, there was no evidence of these fishing activities in the data records. There were no accompanying hydrographic measurements.

The moorings are denoted as A, B, and C in Figure 1. Moorings A, B, and C were deployed on the bottom at depths of 77, 82, and 89 m in the relatively deep trough oriented north to south in the Yellow Sea. Mooring A consisted of a 150 KHz narrowband ADCP, and mooring C consisted of a 300 KHz broadband ADCP, enabling almost full water column profiles. Mooring B consisted of a 1200 KHz narrowband ADCP and thus only profiled 20 m off of the bottom but at a high vertical resolution of 1 m within the bottom boundary layer. The instrument error for moorings A and B is ~1 cm/s and is <1 cm/s for mooring C. Geographical positions, deployment periods, water depths, and ADCP sample levels are provided in Tables 1a and 1b. ADCP sample levels correspond to velocities at the center of the sampling bin, indicated by bin size in Tables 1a and 1b. The depth-dependent structure of the currents and tides is reported on by *Teague et al*. [1998].

Each mooring also contained a PG. Since the pressure of 1 dbar corresponds approximately to the sea pressure exerted by a water column of 1 m, the pressure measurements will be referred to in units of meters. The accuracy of each PG is ~3 cm. Since fluctuations in atmospheric pressure during the passage of storms may result in errors of 5–10 cm in height, atmospheric pressure was removed using the total NOGAPS pressures. NOGAPS wind and pressure data are provided on a $1.25° \times 1.25°$ grid at 0.5 day intervals. The mooring time series of pressure are corrected with the NOGAPS pressure data interpolated to 1 hour intervals at the grid points closest to the mooring locations.

Bottom pressure and profiles of u (east-west) and v (north-south) components of velocity were recorded every 15 min (except every 30 min for the ADCP measurements at mooring A). All three moorings were deployed at about the same time,

Table 1a. ADCP Summary

	Lat., °N	Lon., °E	Start Day	End Day	Depth, m	Bin Size, m
ADCP A	33.267	125.251	183	308	14–70	8
ADCP B	33.750	125.000	184	308	68–87	1
ADCP C	35.967	124.033	213	407	14–72	2

ADCP, acoustic Doppler current profiler.

Table 1b. Pressure Gauge Summary

	Lat., °N	Lon., °E	Start Day	End Day	Water Depth, m
Pressure gauge A	33.267	125.251	183	308	82
Pressure gauge B	33.750	125.000	184	308	89
Pressure gauge C	35.967	124.033	185	324	77

but moorings A and B were recovered about three months before mooring C was recovered. Logging problems resulted in data loss at the beginning of the ADCP record and at the end of the PG record at mooring C. Overall, data return was good. The ADCP records were relatively spike free and required very little editing. The pressure time series has a range of 2.5 m at moorings A and B and over 3.0 m at mooring C. Tides dominate the pressure records. Tides also dominate the current records, and the velocity fields are highly barotropic, with velocities exceeding 50 cm/s [*Teague et al*., 1998].

The temperature sensors are part of the ADCP hardware and have an uncertainty of ±0.4°C. Postcruise calibrations of these sensors were not made. No concurrent hydrographic measurements in conjunction with these measurements were made.

3. Observations

There is a strong seasonal variation in water masses in the Yellow Sea. In lieu of having concurrent hydrographic measurements, mean monthly profiles of temperature are formed using data from Master Oceanographic Observational Data Set (MOODS) [*Teague et al*., 1990], maintained at the Naval Oceanographic Office. Profiles of temperature for July through February are shown in Figure 2. At the southern site A a three-layer hydrographic structure (mixed layer, thermocline, and deep layer) exists from July through October, and a one-layer structure (nearly uniform in temperature from the surface to the bottom) is present from November through February. At the northern site C the deep layer is approximately 5°C cooler. A three-layer structure is present at site C from July through December while a one-layer structure is present in January and February. Erosion of the thermocline begins in October at both locations. Such a large seasonal variation in temperature is related to strong surface cooling in winter and a strong seasonal warming in summer.

Previous analyses of these current measurements [*Teague et al*., 1998] have also identified three layers. Three flow regimes were found during the summer and fall: a near-surface layer (upper 20 m), a middle layer, and a shear layer near the bottom (bottom 10–15 m). These layers appear to be related to the hydrographic structure (Figure 2). During winter the water column is well mixed and can be considered as a single layer from both a hydrographic and current perspective. For comparison with the winds and pressure, top, midlevel, and near-bottom velocity time series are selected at each of the sites. As seen from the climatological profiles in Figure 2, the top level (14 m) is often in or near the mixed layer, the midlevel (38 m at site A and 44 m at site C) is in the thermocline when it exists, and the bottom level (70 m, 72 m, and 87 m for sites A, B, and C, respectively) is below the thermocline for the summer and fall periods. For analyses of the low-frequency mean current flow, tidal currents were removed from the ADCP records by using a low-pass filter with a 40 hour cutoff frequency. The pressure data were similarly filtered in order to remove diurnal and semidiurnal tides.

Current statistics for the detided data consisting of monthly mean current components, standard deviations, minimums, maximums, mean speeds, and directions (0° is north) are provided for sites A, B, and C in Tables 2a–2c. In the surface layer at site A, mean currents were toward the north at ~20 cm/s in July and August and then switched toward the southwest in September and October with mean speeds of 8 and 25 cm/s, respectively (Table 2a). The mean flow calculated over all four months of 6 cm/s toward the northwest is not representative of

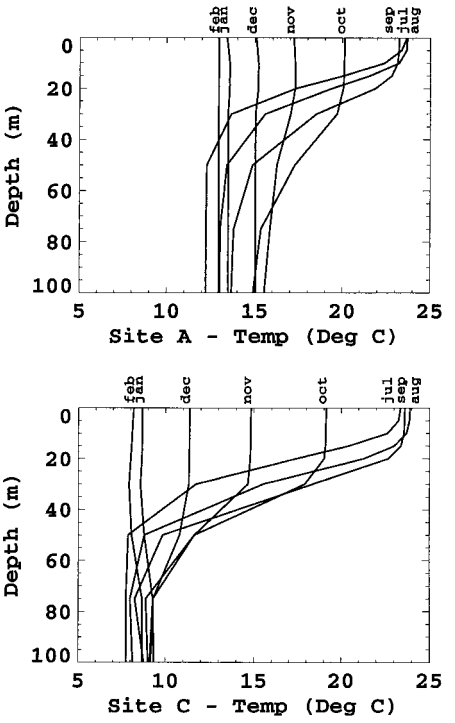

Figure 2. Mean monthly profiles of temperature are shown for July through February. These profiles are formed using data from Master Oceanographic Observational Data Set (MOODS) [*Teague et al*., 1990].

the currents in the near-surface layer at site A. In the midlevel and near-bottom layers at site A, the mean flow for four months is more representative and is ~4 cm/s and 3 cm/s, respectively, toward the northwest. At site B, mean speed in the deep layers generally ranged between 2 and 3 cm/s toward the southeast (Table 2b). Overall mean currents at the northern site C are ~1 cm/s, toward the southeast at the near-surface level but toward the northeast at the midlevel and near-bottom level (Table 2c). Currents are smaller at the northern site C than at the southern site A. Maximum monthly mean current speed among all three sites is 25 cm/s toward the southwest at the near-surface level at site A in October.

The mooring time series of current and pressure are compared with the wind data from NOGAPS at the grid points closest to the mooring locations. The filtered current and pressure data are subsampled at 0.5 day intervals for comparison with NOGAPS winds. Note that the NOGAPS wind field is the same for sites A and B because of their close geographical proximity. Vector stick diagrams of current velocities and wind stress and pressure time series are presented in Figures 3–5. The summer monsoon period with south winds extends until about day 245 (September 2). A fall transition period with mainly light north winds follows and continues until day 303 (October 30). The winter monsoon period then begins with strong north wind pulses and continues through the end of the measurement period. Monthly mean wind stress and direction are provided in Table 3. Current measurements are obtained for the months of July through October for sites A and B and for the months of August through February for site C.

At site A (Figure 3), currents in the near-surface layer (14 m) respond quickly to the wind stress and tend to flow toward the north with south winds and toward the south with north

Table 2a. Current Statistics: ADCP A

Month	Depth, m	$\bar{u}$	σ_u	$u_{\min}$	$u_{\max}$	$\bar{v}$	σ_v	$v_{\min}$	$v_{\max}$	$\overline{S_p}$	Dir
All	14	−4.6	18.2	−48.4	42.8	4.1	23.8	−46.1	46.1	6.1	312
July	14	2.8	14.6	−35.5	31.2	21.8	14.9	−29.8	38.1	21.9	7
Aug.	14	2.0	14.6	−39.2	27.7	21.8	9.1	−2.7	34.3	21.9	5
Sept.	14	−6.2	20.3	−43.5	42.8	−5.5	19.3	−34.9	46.1	8.3	228
Oct.	14	−15.9	16.1	−48.4	22.2	−19.6	17.4	−46.1	44.5	25.3	219
All	38	−2.9	5.8	−15.8	13.9	2.4	5.1	−7.6	23.3	3.8	310
July	38	−1.9	3.2	−7.8	6.4	2.0	3.4	−7.6	7.1	2.8	317
Aug.	38	−8.2	4.9	−15.8	3.3	0.2	3.4	−5.1	10.2	8.2	271
Sept.	38	0.2	4.7	−8.3	9.5	5.1	5.9	−6.8	15.1	5.1	3
Oct.	38	−1.7	5.9	−11.4	13.9	2.4	5.7	−6.9	23.3	3.0	325
All	70	−2.8	2.3	−9.4	2.7	1.2	3.2	−6.4	9.7	3.0	293
July	70	−1.8	2.0	−7.5	2.7	1.4	3.0	−6.4	6.1	2.3	308
Aug.	70	−2.1	1.6	−5.6	1.6	0.3	2.8	−5.5	8.4	2.2	279
Sept.	70	−2.7	2.6	−8.9	2.7	2.4	3.5	−4.0	8.5	3.6	312
Oct.	70	−4.3	1.9	−9.4	0.6	0.7	3.3	−5.7	9.7	4.4	279

Current statistics are given in cm/s. Parameters are as follows: $\bar{u}$ and $\bar{v}$, mean east-west and north-south components of velocity, respectively; $\overline{S_p}$, mean current speed. Dir, current direction (where 0° is north). All, calculated over all four months.

winds. Current directions for the mean monthly currents (Table 2a) in the near-surface layer at site A are similar to the directions of the monthly mean wind stresses (Table 3a). Northward currents and south winds are found in July and August while southward currents and north winds are found in September and October. Current directions in the middle and near-bottom layers are toward the northwest and have mean velocities of approximately 3 cm/s. The current directions in the lower layers do not generally reflect the wind direction. Expanded views of the near-surface, mid-level, and near-bottom flows at sites A, B, and C (all denoted by thin lines which are solid, dashed, and dash-dotted, respectively) are shown with wind stress (thick sold line) and bottom pressure (thick dashed line) in Figure 6. Near the end of the measurement period (day 303) at site A, the strongest north wind burst is measured, and the midlevel and lower level both respond with a strong northward flow of ~20 cm/s at ~1.5 days phase lag with the winds (Figure 6a). The near-surface layer responds similarly with a reversal from a southward flow of ~15 cm/s to a very small northward flow of 1 cm/s at a similar phase lag. A large pressure anomaly lags the north wind burst at day 303 by ~1/2 day. The differences in current response could be due to a background sea surface slope forming during the later wind burst period.

Only bottom layer velocities are recorded at site B (Figure 4). Bottom layer velocities are very similar to each other but quite different from the bottom velocity at site A. At site B the mean near-bottom velocity is ~2 cm/s toward the southeast (Table 2b). There is an isolated north wind burst near day 203 in which there is a northward flow response at depth. In contrast, there is a south wind burst near day 237 which is followed by a northward flow response. The intense north wind burst near day 303 is followed by strong northward flow of almost 20 cm/s, decreasing in magnitude toward the bottommost layer (Figure 6b). The pressure record indicates a reduction in sea level near day 303 as also observed at site A. The fact that the pressure records at sites A and B are so similar increases our confidence in using the same wind field for both sites.

At site C (Figure 5) the winds also switch to toward the south at day 245 and continue mainly out of the north through the end of the measurement period (day 405, February 9). The magnitude of the winter monsoon wind stresses is about double the magnitude of the summer wind stresses. Fluctuations in the pressure time series approximately double during the winter monsoon. The large pressure fluctuations trail the strong north wind events by ~1–2 days. Current directions for the mean monthly currents (Table 2c) at the near-surface level at

Table 2b. Current Statistics: ADCP B

Month	Depth, m	$\bar{u}$	σ_u	$u_{\min}$	$u_{\max}$	$\bar{v}$	σ_v	$v_{\min}$	$v_{\max}$	$\overline{S_p}$	Dir
All	68	1.4	3.7	−11.0	10.9	−2.1	4.0	−13.7	8.0	2.5	146
July	68	−0.7	2.6	−6.7	5.8	−3.8	3.8	−13.7	2.6	3.9	190
Aug.	68	2.4	2.9	−4.9	7.7	−2.7	4.5	−12.8	8.0	3.6	138
Sept.	68	0.6	4.3	−11.0	9.3	−0.7	4.0	−11.8	5.9	0.9	138
Oct.	68	2.9	3.7	−5.2	10.9	−1.4	2.6	−7.4	5.1	3.2	117
All	77	1.7	3.2	−7.8	8.5	−1.8	3.7	−11.8	7.4	2.5	136
July	77	0.5	3.0	−6.8	6.3	−3.7	3.4	−11.8	2.0	3.8	173
Aug.	77	3.0	2.8	−3.8	8.1	−2.4	4.4	−11.3	7.4	3.8	128
Sept.	77	0.8	3.2	−7.8	8.5	−0.2	3.4	−11.1	5.4	0.8	103
Oct.	77	2.3	3.2	−6.6	8.0	−1.1	2.4	−5.8	6.0	2.5	115
All	87	1.5	2.7	−6.7	8.1	−1.3	3.2	−10.5	6.2	2.0	132
July	87	1.0	2.9	−6.7	5.7	−3.1	3.1	−10.5	2.1	3.2	163
Aug.	87	2.6	2.6	−2.8	8.1	−1.8	4.0	−9.8	6.2	3.1	125
Sept.	87	0.6	2.4	−4.2	7.1	0.3	2.5	−6.7	4.5	0.7	61
Oct.	87	1.6	2.5	−5.6	6.7	−1.0	1.9	−4.7	5.1	1.9	122

Current statistics are given in cm/s.

Table 2c. Current Statistics: ADCP C

Month	Depth, m	$\bar{u}$	σ_u	$u_{\min}$	$u_{\max}$	$\bar{v}$	σ_v	$v_{\min}$	$v_{\max}$	$\overline{S_p}$	Dir
All	14	1.1	6.0	−17.1	33.8	−0.5	6.9	−23.4	21.3	1.2	116
Aug.	14	2.6	5.7	−14.5	16.9	4.4	5.2	−12.9	14.2	5.1	30
Sept.	14	2.5	2.6	−7.1	7.1	−1.4	4.1	−17.0	6.1	2.8	119
Oct.	14	−0.2	3.8	−11.8	8.8	−1.7	5.2	−17.4	8.6	1.8	186
Nov.	14	−0.0	6.1	−17.1	16.3	0.3	8.2	−23.0	21.3	0.3	359
Dec.	14	0.3	11.0	−13.7	33.8	−1.1	8.6	−23.4	15.9	1.2	165
Jan.	14	1.6	3.5	−5.6	9.7	−3.1	6.5	−20.3	13.1	3.5	153
Feb.	14	0.7	2.5	−5.4	5.6	−1.1	6.7	−12.8	11.6	1.3	147
All	44	0.6	4.4	−12.0	24.7	1.1	5.4	−18.5	19.2	1.2	28
Aug.	44	−0.9	1.9	−8.3	2.7	0.9	4.2	−15.2	9.0	1.2	315
Sept.	44	0.1	1.8	−4.7	4.2	0.6	2.3	−6.6	6.0	0.6	12
Oct.	44	1.1	2.1	−4.0	7.6	0.3	2.5	−4.5	13.1	1.2	74
Nov.	44	2.0	5.1	−8.0	15.2	3.0	7.2	−14.3	19.2	3.6	34
Dec.	44	0.0	8.4	−12.0	24.7	3.9	6.0	−9.6	18.4	3.9	0
Jan.	44	1.1	2.4	−3.6	7.1	−1.8	5.4	−18.5	13.1	2.2	148
Feb.	44	0.0	2.2	−5.7	4.2	0.1	6.3	−11.3	13.1	0.1	6
All	72	0.4	2.8	−8.3	12.7	1.3	3.6	−14.3	13.0	1.3	20
Aug.	72	−0.5	1.7	−3.9	4.0	0.5	3.8	−14.3	7.0	0.7	318
Sept.	72	0.6	1.6	−3.3	5.9	0.7	1.6	−4.3	3.6	0.9	44
Oct.	72	0.9	1.7	−3.8	6.0	0.1	1.9	−3.1	8.8	0.9	85
Nov.	72	0.2	3.8	−8.3	9.7	2.2	3.9	−5.4	12.8	2.3	4
Dec.	72	0.4	3.1	−7.1	10.7	3.9	3.1	−2.6	10.2	3.9	5
Jan.	72	1.3	3.5	−5.5	12.7	0.3	3.9	−6.5	13.0	1.4	76
Feb.	72	−0.5	2.3	−5.1	3.6	0.7	5.3	−8.9	11.9	0.8	325

Current statistics are given in cm/s.

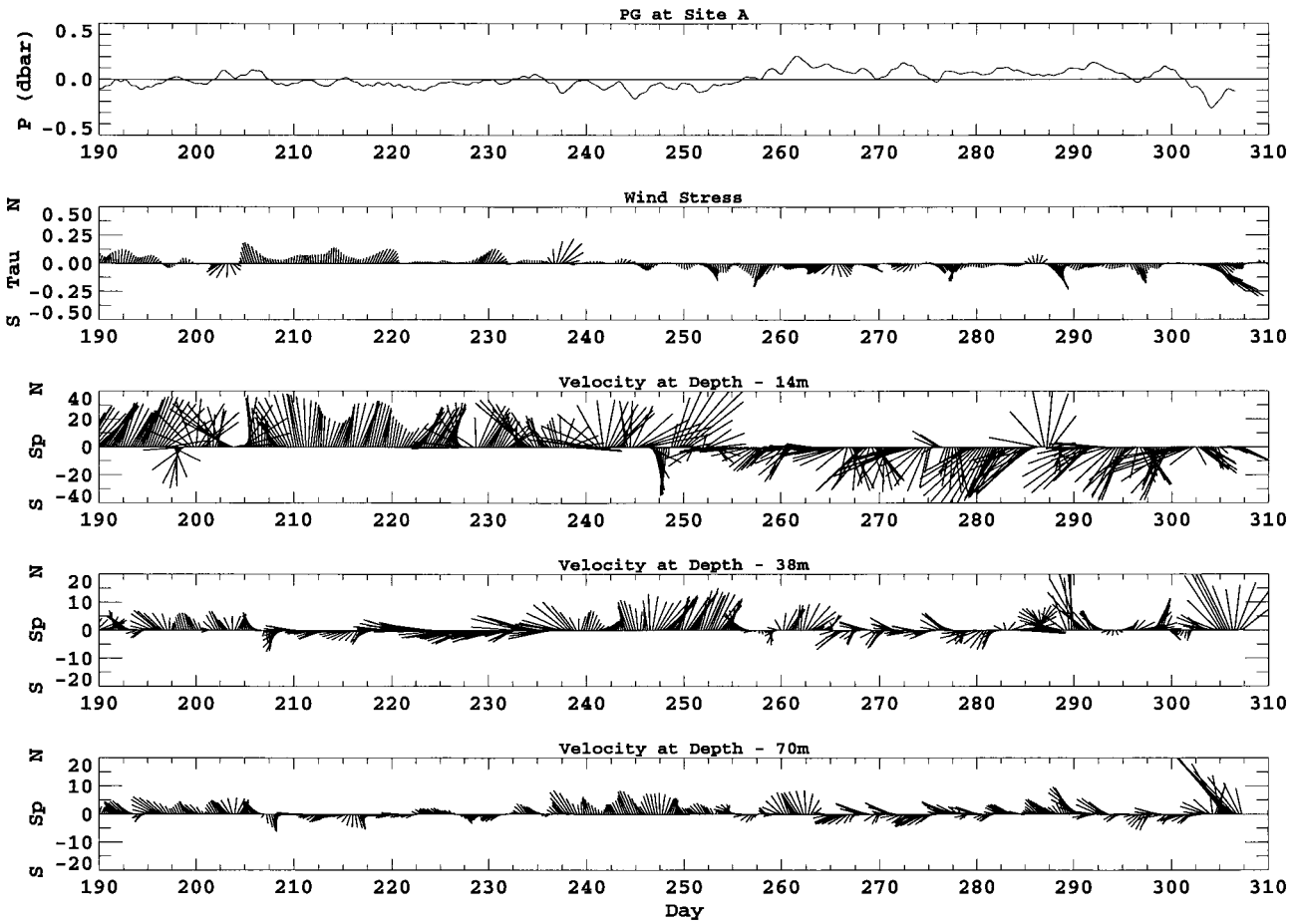

Figure 3. Pressure anomaly and vector stick diagrams of wind stress and current velocities at 14, 38, and 70 m for site A. The currents have been filtered to remove tides.

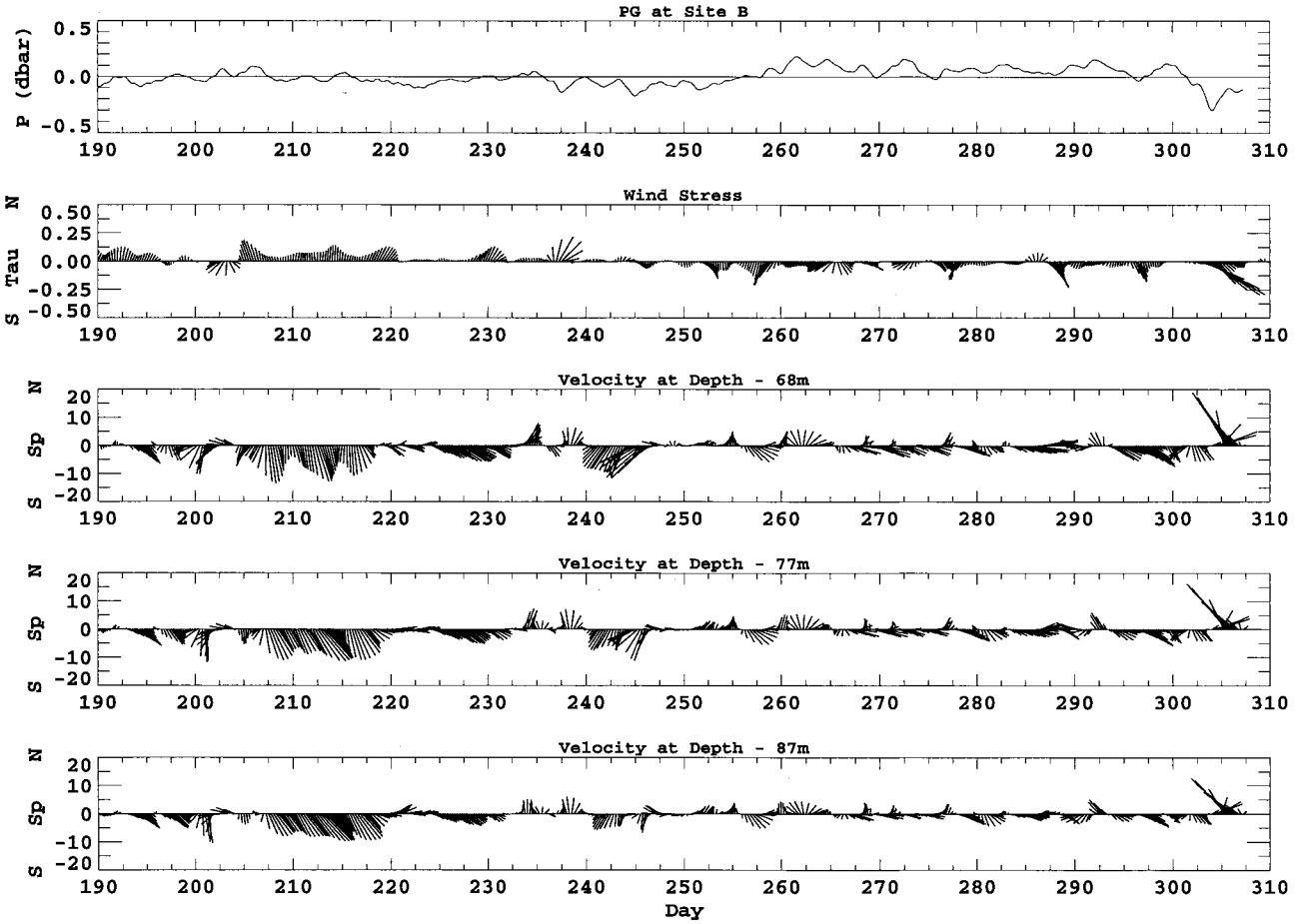

Figure 4. Pressure anomaly and vector stick diagrams of wind stress and current velocities at 68, 77, and 87 m for site B. The currents have been filtered to remove tides.

site C are similar to the directions of the monthly mean wind stresses (Table 3b). Current flows at the middle and near-bottom levels are generally toward the north, opposite to the direction of the wind. Particularly strong wind events near days 303, 357, 367, 372, and 396 are followed by relatively strong northward current bursts at each of the three depth levels (Figures 6c–6f). During periods when the north wind relaxes somewhat, current flow is often toward the south at the top and middle levels (Figure 5b; days 347–357 and days 382–395, for example). The fast reversal of currents indicates the presence of a background slope which is in opposition to the slop set up by the winter monsoon. During January and February (days 365–405) at site C, the water column is well mixed from the surface to the bottom (Figure 2), and the current response was similar to each depth level (Figure 5b).

Bottom temperature is shown for all three sites in Figure 7. Bottom temperatures at site A are warmer than at site B, which is located to the north of site A (Figure 1). Since warmer waters from the south do not flow as far north as site B, a clockwise steering of the warmer Tsushima Current waters along the bathymetry contours around Cheju is probable. Temperature records at both sites A and B reflect a sharp rise in temperature (2° and 1°, respectively) at day 305, near the time of the north wind burst and associated northward current flow. At site C, which is approximately 2° in latitude north of sites A and B, a much slower rise in temperature begins around day 288 (October 15), continuing to rise until day 365 and then falling at day 375 (January 10) to temperatures below the temperature at the beginning of the rise. The warmer water between days 288 and 375 results from transport of warmer water from the south, and not necessarily Tsushima Current waters. Temperature records at site C indicate cold water anomalies originating near days 215 and 240 and suggest a southward current flow. Current measurements are not available for day 215, but a southward flow is found near day 240 (Figure 5a). Cessation of the warm temperature rise at day 375 does not mean that water from the south has stopped but rather that the southern waters have cooled off and that the entire area is becoming more isothermal.

A hypothesis proposed by *Hsueh* [1988] is that the northward current bursts in the Yellow Sea trough are forced by a north-to-south pressure gradient associated with north wind pulses. Figure 8 shows plots of atmospherically corrected pressure anomaly at site A minus the atmospherically corrected pressure anomaly at site C and of the atmospherically corrected sea level height at Mokpo minus the corrected sea level height at Anhung. A positive anomaly indicates a rise in sea level toward the south. A large positive pressure anomaly is indicated in the pressure differences between sites A and C near day 303, which correspond to the rise in temperature, north wind pulse, and north current burst. Given a longer time series, a negative anomaly would be apparent prior to day 300. A clear positive anomaly between Mokpo and Anhung occurs near day 277 (October 4) and continues through day 375, where negative anomalies be-

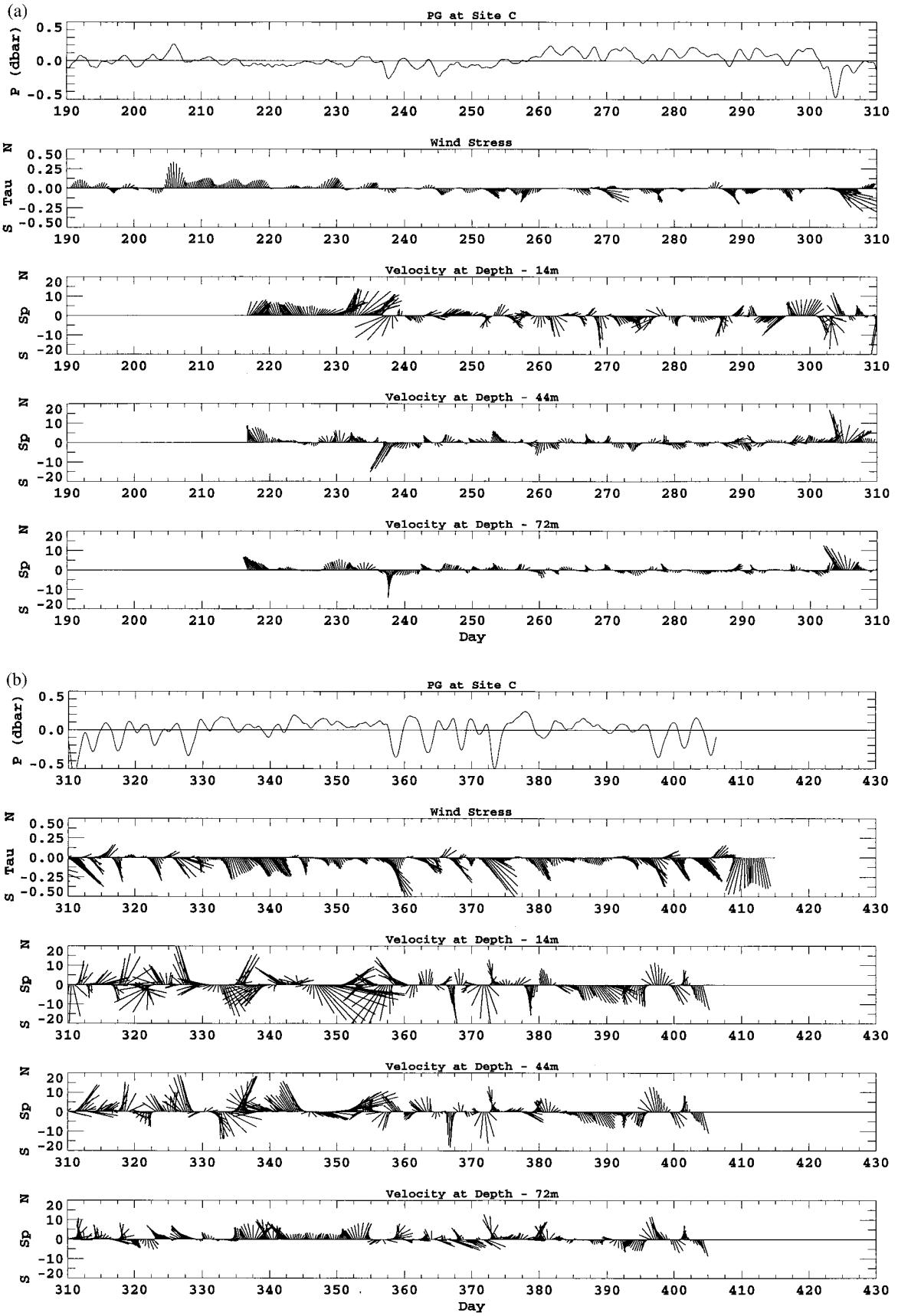

Figure 5. (a) Pressure anomaly and vector stick diagrams of wind stress and current velocities at 14, 44, and 72 m for site C (day 190–310, July–November). The currents have been filtered to remove tides. (b) Pressure anomaly and vector stick diagrams of wind stress and current velocities at 14, 44, and 72 m for site C (day 310–410, November–February). The currents have been filtered to remove tides.

Table 3a. Mean Wind Stress: Sites A and B

Month	Wind Stress, n/m^2	Direction
July	0.041	3
Aug.	0.046	20
Sept.	0.052	190
Oct.	0.060	160

Table 3b. Mean Wind Stress: Site C

Month	Wind Stress, n/m^2	Direction
Aug.	0.036	26
Sept.	0.044	149
Oct.	0.066	139
Nov.	0.112	132
Dec.	0.148	146
Jan.	0.110	139
Feb.	0.187	157

gin to be interspersed with the positive anomalies. This suggests that the north wind is more effective in driving up the sea level in the shallow waters near the coast.

4. Spectral Analyses

For quantitative comparisons of the currents and the winds, spectra are computed. In computing the spectra the time series are broken into 30 day segments and overlapped by 15 days. The spectrum of each segment is computed, and the resulting spectra are averaged. At the mooring locations the current, pressure, and wind stress data all indicate local spectral maxima in bands centered on weekly and semiweekly periods. Overall energy is higher in pressure at site C than at site A while the energy is higher in the near-surface current (14 m) at site A. The pressure and wind spectra for site C contain significant peaks near 0.13 cycles per day (cpd) and 0.3 cpd (7.7 day, or weekly, and 3.3 day, or semiweekly, periods). Similar peaks at site C are found in the near-surface north-south velocity (14 m), but only the semiweekly peak is found at middepth (44 m) and near the bottom (72 m). At mooring A, peaks in the spectra are less distinctive but similar to those at mooring C. At both moorings A and C, semiweekly variability is larger than the weekly variability. The variability at the weekly and semiweekly bands indicates a link between the local wind forcing and the currents.

Cross spectra are computed and analyzed for various combinations of velocity, wind, and pressure. The phase and coherence for some of these combinations are shown in Figure 9. The 95% significance limit is plotted on the coherence of the cross spectra. Coherences are meaningful down to periods of ~2 days (0.5 cpd). At the near-surface level, low but significant coherence (0.7) is found between velocity and wind stress at site A while high coherence (0.9) is found between velocity and wind stress at site C for semiweekly periods. At middepth at sites A and C, coherence and phase for the north-south component of velocity v at 38 m and wind τ_y display high coherences (>0.8) for semiweekly periods (Figures 9a and 9b). High coherence (0.8) between wind stress and pressure for both weekly and semiweekly periods is found at site C (Figure 9c)

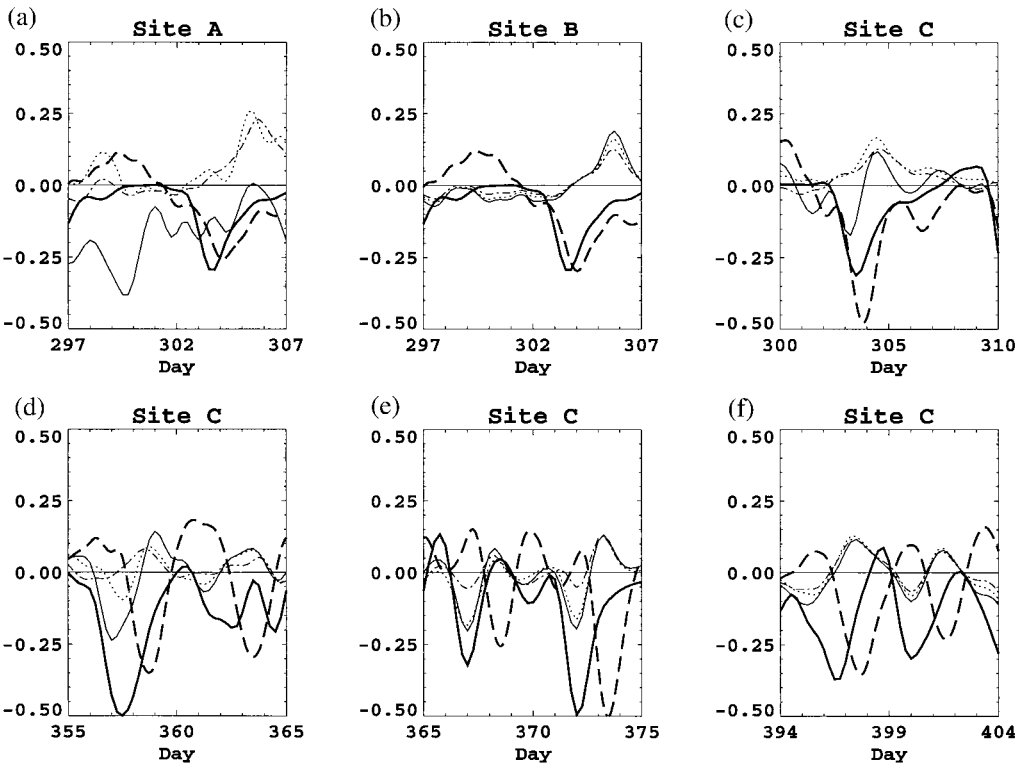

Figure 6. North-south component of the wind (solid line), pressure (dashed thick line) and north-south velocity components for the top (thin line), mid-level (dashed line), and near-bottom (dash-dotted line) levels for selected 10 day periods: (a) at site A (14, 38, and 70 m), (b) at site B (68, 77, and 87 m), and (c–f) at site C (14, 44, and 72 m). Units for the y axis are in m/s for currents, dbar for pressure, and n/m^2 for wind stress.

while low coherence between wind stress and pressure is found at sites A and B. Near the bottom, high coherence (0.85) is found between velocity and wind stress for the semiweekly periods at sites A and C while low coherence is found at the nearby site B. Since sites A and B are very close geographically, different driving mechanisms are suggested for the deep currents between these two locations.

From the phase lag at a particular frequency where there is significant coherence, the difference in time response between the two series can be calculated. For example, a phase of $-90°$ at 0.3 cpd (3.3 day period) between v and τ_y corresponds to v lagging behind τ_y by one-quarter period or 0.83 days. At site A the v velocity component at the near-surface levels trails τ_y wind component by only ~0.4 days at the weekly and semiweekly periods while at middepth and near-bottom levels the v velocity component trails τ_y wind component by 1–2 days at the semiweekly periods and weekly periods. At site C, higher coherences are found between the wind and current, and the v velocity component trails τ_y wind component by ~1.5 days at semiweekly periods and by ~2.5 days at weekly periods. Wind stress lags the pressure by about a day at the weekly periods at site C.

Cospectral analysis of the north-south components of velocity between ADCP A and C (Figure 10) indicates a significant coherence in the semiweekly band and corresponds to a northward phase propagation at speeds of the order of 200 km/d,

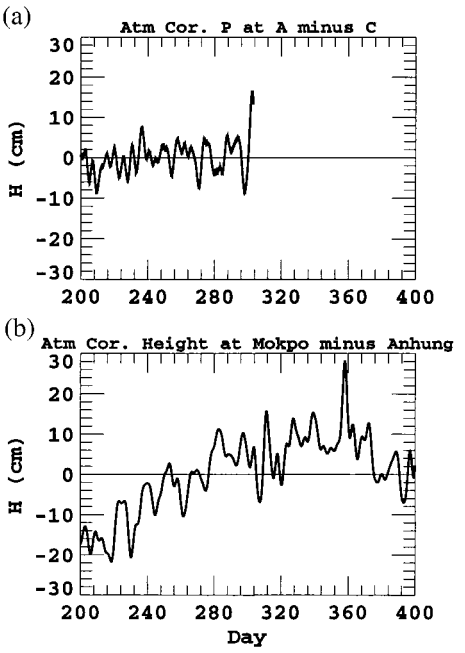

Figure 8. (a) Atmospherically corrected pressure at site A minus the corrected pressure at site C. (b) Atmospherically corrected height from tide gauge measurements at Mokpo minus the corrected height from tide gauge measurements at Anhung.

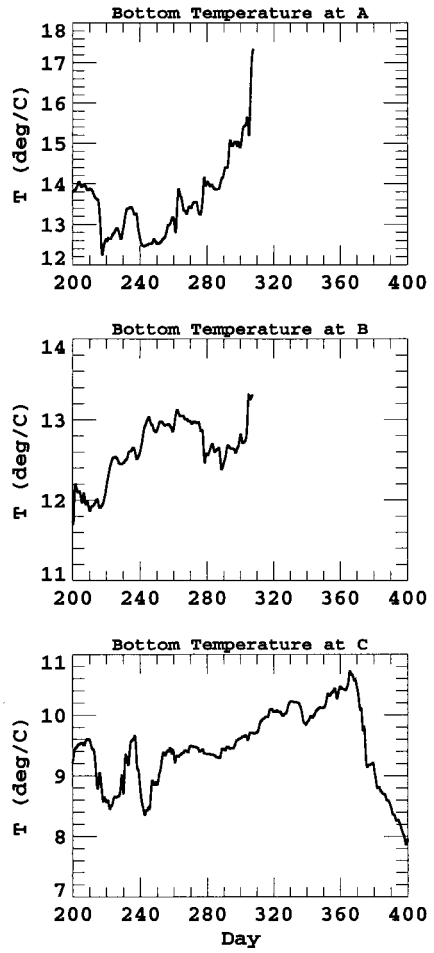

Figure 7. Bottom temperature at sites A, B, and C.

about one third of the propagation speed calculated by *Hsueh* [1988] but still a a reasonable value for continental shelf waves in the Yellow Sea trough [*Hsueh and Pang*, 1989]. *Hsueh* [1988] observed phase speeds of the order of 500 km/d during the winter months (January–March) and attributed their existence to the winter monsoon wind events. Our measurements were made primarily during late summer and fall and are also related to wind events.

5. Discussion

Understanding the wind stresses and pressure gradients can lead to a better understanding of the YSWC variations. *Jacobs et al*. [1998] examined the sea surface height (SSH) variability in the Yellow and East China Seas using TOPEX/Poseidon altimeter data, winds, two models, and the pressure gauge data described here and found weekly and semiweekly variability, in the SSH. The spatial variability in the SSH is similar to the wind stress variability, which is dominated by weekly and semiweekly events. The current response lags the wind field by 1–2 days below the near-surface layer. In the near-surface layer the response may be much less than a day. Such forcing events can cause unevenly spaced current pulses. During the winter, *Hu* [1994] suggests that the Yellow Sea Warm Current (YSWC) is a warm subsurface current that is sporadically driven northward from the Tsushima Current. An intermittent Yellow Sea Warm Current (YSWC) has been observed in the ADCP records presented here (July–February). Northward drift forced by south winds is observed during summer. Beginning in early November (day 305), there is a northerly current flow response to north wind pulses. At the southern sites A and B this type of response is found in the middle and near-bottom layers (Figures 3 and 4). However, it occurs over almost the entire water column at site C, from the uppermost velocity bin

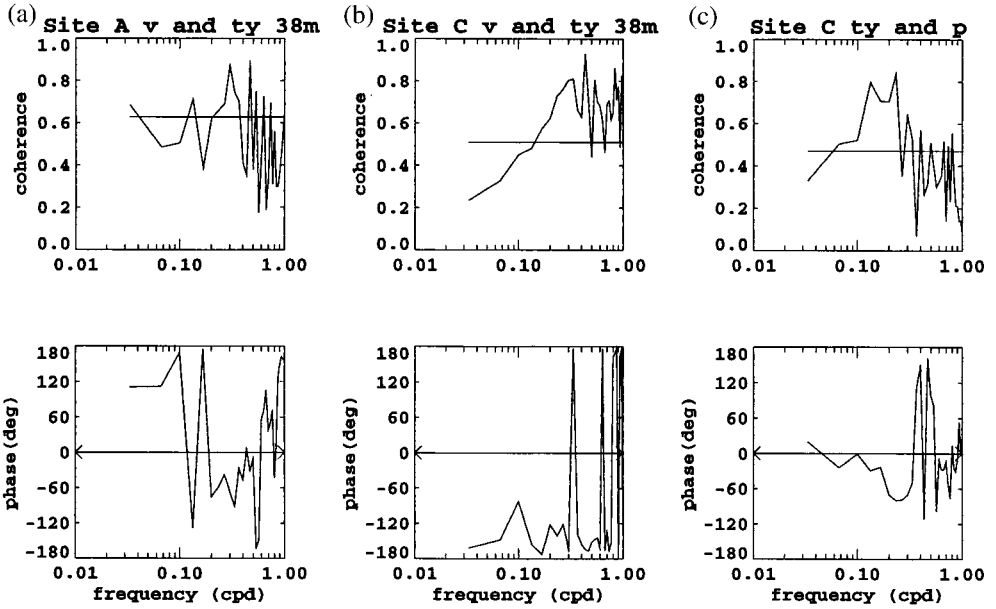

Figure 9. (a) Coherence and phase diagrams for the north-south component of current velocity v for middepth (38 m) and north-south component of wind stress τ_y at site A. (b) Same as for Figure 9a but for site C. (c) Coherence and phase diagrams for the north-south component of wind stress and pressure at site C. The 95% confidence level is indicated. Negative phase indicates that the currents trail the wind and that the wind stress trails the pressure fluctuations.

at 14 m to the velocity bin at 72 m. The wind pulses have a duration of ~3 days to one week. During periods where the wind relaxes and weakens, southward current flow is found at the upper and middle levels (Figure 5b; day 350) and at all levels (day 385) at site C. Southward current flow between two closely spaced north wind bursts is seen near days 400 and 404 at site C (Figure 5b). Hence the current flow is not continually toward the north throughout the winter. The vertical structure of the current velocity appears to be closely linked to the hydrographic structure, with both currents and hydrography consisting of multiple layers during summer and fall and only a single layer during the winter. These data provide evidence that the YSWC is correlated to the meridional pressure gradient induced by the wind stress. *Hsueh* [1988] presented evidence that this event results from the winter monsoon winds from measurements made during the months of January–April. Here, measurements are presented that show that the YSWC is forced by north winds during the fall transition period, continuing into the winter monsoon, and is forced by south winds during the summer. This northward flow can certainly transport warmer and more saline waters from the south and may advect waters of Kuroshio origin.

The drift at 70 m at site A is toward the northwest along the bathymetry contours, opposite to southeastward drift observed at site B, also along the bathymetry contours. Bottom temperature records at site B (Figure 7) show a rise in temperature and suggest that the southeastward flow may have a southern source. Deep temperatures observed at site A are warmer than the deep temperatures observed at site B. Since the temperature observation depths are similar and site B is north of site A, a clockwise turning of the flow along the bathymetry toward the east between Cheju and southwestern Korea is suggested. From analyses of extensive hydrographic data collected in 1982 and 1983, *Park* [1986] points out that in the summer the warm and saline water of Kuroshio origin flows into the Cheju Strait after flowing around the west coast of Cheju Island. He found that water of probable Kuroshio origin (salinity greater than 34.0) surrounded Cheju and found no salinities greater than 33.5 north of the southeastern entrance of the Yellow Sea. Similar hydrographic conditions are also found by *Lie* [1985, 1986]. The eastward turning of the YSWC around Cheju has been observed in other years and may be typical. Some previous current measurements support a northward flow of the YSWC near the west coast of Cheju and its eastward turning

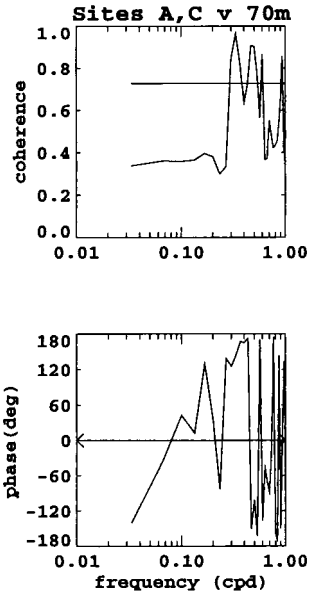

Figure 10. Coherence and phase for the north-south components of velocity at 70 m between sites A and C. The 95% significance level is indicated.

into the Cheju Strait [*Kim*, 1979; *Kim et al*., 1991]. *Lee and Bong* [1969] concluded from a drift bottle experiment that eastward flow exists along the north coast of Cheju throughout the year. More recently, *Lie et al*., [1998] analyzed 172 satellite-tracked drifters which were deployed near Taiwan and in the eastern East China Sea and found that not a single drifter penetrated into the Yellow Sea. One of the drifters travelled clockwise around Cheju. A direct branching of the Tsushima Current into the Yellow Sea does not occur.

6. Conclusions

There is likely a year-round northward flow driven by several mechanisms along the Yellow Sea trough. Although temperature and salinity values characteristic of Kuroshio waters have been observed in the Yellow Sea interior, this analysis of direct current observations suggests that this warmer, saltier water is due to advection by wind-driven sporadic current events. The northward flow, observed in the deeper layers during fall and throughout the water column during winter, is certainly not due to a branching of the Tsushima Current but is rather a response to a pressure gradient set up by north monsoon winds. This type of current response, directly observed by these measurements, is found to begin at the onset of the winter monsoon in late October. Northward flow near the surface during summer and southward flow near the surface in fall are apparently a direct response to the south and north winds, respectively, in the highly stratified water. The vertical structure of the current field is related to the hydrographic structure. The deeper flows are affected by wind, pressure, stratification, and bathymetric influences, but more measurements are needed to fully understand the deep flows.

What is now known as the YSWC could actually be three currents. The branching of the Tsushima may only extend to the north as far as the Cheju vicinity. Direct observations of a southeastward flow near the bottom and temperature variation northwest of Cheju are suggestive of a clockwise flow around Cheju. Northward drift in the Yellow Sea during the summer is highly correlated with the south winds. Northward flow in the fall and winter in the Yellow Sea interior is a response to the pressure gradient set up by the north monsoon winds. Perhaps a better name for the YSWC in the interior of the Yellow Sea might be the Yellow Sea Wind Current.

Acknowledgments. Thanks are extended to the following personnel at the U.S. Naval Oceanographic Office: to Craig Cumbee and Pete Heuser for outstanding work in the deployment and recovery operations, to John Blaha for his helpful suggestions, and to Stan Raffa, whose resource planning made this work possible. We are grateful to Kyung-Il Chang of KORDI for providing tide gauge data along the west coast of Korea. This work was supported by the Office of Naval Research as part of the Basic Research Project "Yellow and East China Seas Experiment" under Program Element 601153N (NRL-SSC contribution 7332-97-0041).

References

Asaoka, O., and S. Moriyasu, On the circulation in the East China Sea and the Yellow Sea in winter (Preliminary Report), *Oceanogr. Mag*., *18*, 73–81, 1966.

Beardsley, R. C., R. Limeburner, H. Yu, and G. A. Cannon, Discharge of the Changjiang (Yangtze River) into the East China Sea, *Cont. Shelf Res*., *4*, 57–76, 1985.

Chen, C., R. C. Beardsley, R. Limeburner, and K. Kim, Comparison of winter and summer hydrographic observations in the Yellow and East China Seas and adjacent Kuroshio during 1986, *Cont. Shelf Res*., *14*, 909–929, 1994.

Cumbee, S. A., and J. M. Foley Jr., Naval Oceanographic Office's first operational use of trawl-resistant packages housing acoustic doppler profilers, *Oceans*, *2*, 1372–1380, 1995.

Hogan, T. F., and L. R. Brody, Sensitivity studies of the Navy global forecast model parameterizations and evaluation of improvements to NOGAPS, *Mon. Weather Rev*., *121*(8), 2373–2395, 1993.

Hogan, T. F., and T. E. Rosmond, The description of the Navy Operational Global Atmospheric Prediction System, *Mon. Weather Rev*., *119*(8), 1786–1815, 1991.

Hsueh, Y., Recent current observations in the eastern Yellow Sea, *J. Geophys. Res*., *93*, 6875–6884, 1988.

Hsueh, Y., and I. C. Pang, Coastally trapped long waves in the Yellow Sea, *J. Phys. Oceanogr*., *19*(5), 612–625, 1989.

Hu, D. X., Some striking features of circulation in the Huanghai Sea and East China Sea, *Oceanol. China Seas*, *1*, 27–38, 1994.

Jacobs, G. A., W. J. Teague, S. K. Riedlinger, and R. H. Preller, Sea surface height variations in the Yellow and East China Seas, 2, SSH variability in the weekly and semiweekly bands, *J. Geophys. Res*., *103*, 18,479–18,496, 1998.

Kim, B. K., A study on the currents in the Chenju Strait, *Bull. Fish. Res. Devel. Agency*, *21*, 7–21, 1979.

Kim, K., H. K. Rho, and S. H. Lee, Water masses and circulation around Chenju-do in summer, *J. Oceanol. Soc. Korea*, *26*, 262–277, 1991.

Kondo, M., Oceanographic investigations of fishing grounds in the East China Sea and the Yellow Sea, I, Characteristics of the mean temperature and salinity distributions measured at 50 m and near the bottom, *Bull. Seikai Reg. Fish. Res. Lab*., *62*, 19–66, 1985.

Lee, C. K., and J. H. Bong, A study on the surface current of the Korea southern sea by drift bottle experiments, *Bull. Fish. Res. Devel. Agency*, *4*, 45–58, 1969.

Lie, H.-J., A note on water masses and general circulation in the Yellow Sea (Hwanghae), *J. Oceanol. Soc. of Korea*, *19*, 187–194, 1984.

Lie, H.-J., Wintertime temperature-salinity characteristics in the southeastern Hwanghae (Yellow Sea), *J. Oceanogr. Soc. Jpn*., *41*, 291–298, 1985.

Lie, H.-J., Summertime hydrographic features in the southeastern Hwanghae, *Prog. Oceanogr*., *17*, 229–242, 1986.

Lie, H.-J., C.-H. Cho, and J.-H. Lee, Separation of the Kuroshio water and its penetration onto the continental shelf west of Kyushu, *J. Geophys. Res*., *103*, 2963–2976, 1998.

Nakao, T., Oceanic variability in relations to fisheries in the East China Sea and the Yellow Sea, *J. Facu. Mar. Sci. Technol. Tokai Univ*., *11*, 362, pp. 1977.

Nitani, H., Beginning of the Kuroshio, In *Kuroshio: Physical Aspects of the Japan Current*, edited by H. Stommel and K. Yoshida, pp. 129–156, Univ. of Wash. Press, Seattle, 1972.

Park, Y. H., Water characteristics and movements of the Yellow Sea Warm Current in summer, *Prog. Oceanogr*., *17*, 243–254, 1986.

Rosmond, T. E., The design and testing of the Navy Operational Global Atmospheric Prediction System, *Weather Forecasting*, *7*(2), 262–272, 1992.

Teague, W. J., M. J. Carron, and P. Hogan, A comparison between the Generalized Digital Environmental Model and Levitus climatologies, *J. Geophys. Res*., *95*, 7167–7183, 1990.

Teague, W. J., H. T. Perkins, Z. R. Hallock, and G. A. Jacobs, Current and tide observations in the southern Yellow Sea, *J. Geophys. Res*., *103*, 27,783–27,793, 1998.

Uda, M., The results of simultaneous oceanographical investigations in the Japan Sea and its adjacent waters in May and June, 1932, *J. Imperial Fish. Exped. Stns*., *5*, 57–190, 1934.

G. A. Jacobs and W. J. Teague, Naval Research Laboratory, Stennis Space Center, MS 39529-5004. (jacobs@nrlssc.navy.mil; teague@wjt.nrlssc.navy.mil)

(Received October 14, 1998; revised September 21, 1999; accepted October 14, 1999.)